Research Square

Preprints are preliminary reports that have not undergone peer review.
They should not be considered conclusive, used to inform clinical practice,
or referenced by the media as validated information.

Functional analysis of the *Aspergillus fumigatus* kinome reveals a DYRK kinase involved in septal plugging is a novel antifungal drug target

Norman van Rhijn
University of Manchester https://orcid.org/0000-0001-6722-2757
Can Zhao
Manchester Fungal Infection Group
Narjes Al-Furaji
Manchester Fungal Infection Group
Isabelle Storer
University of Manchester
Clara Valero
Manchester Fungal Infection Group
Sara Gago
University of Manchester https://orcid.org/0000-0002-7027-4598
Harry Chown
University of Manchester https://orcid.org/0000-0002-5331-4711
Clara Baldin
Innsbruck Medical University
Rachael Fortune-Grant
Manchester Fungal Infection Group
Hajer Bin Shuraym
Manchester Fungal Infection Group
Lia Ivanova
Leibniz Institute for Natural Product Research and Infection Biology
Olaf Kniemeyer
Leibniz Institute for Natural Product Research and Infection Biology
Thomas Krüger
Leibniz Institute for Natural Product Research and Infection Biology
Elaine Bignell
Manchester Fungal Infection Group
Gustavo Goldman
Faculdade de Ciências Farmacêuticas de Ribeirão Preto, Bloco Q, Universidade de São Paulo
https://orcid.org/0000-0002-2986-350X

Jorge Amich
Instituto de Salud Carlos III https://orcid.org/0000-0002-8987-5115
Daniela Delneri
University of Manchester
Paul Bowyer
University of Manchester https://orcid.org/0000-0002-1083-9286
Axel Brakhage
Leibniz Institute for Natural Product Research and Infection Biology - University of Jena
Hubertus Haas
Institute of Molecular Biology/Biocenter, Innsbruck Medical University https://orcid.org/0000-0003-2472-9878
Michael Bromley
mike.bromley@manchester.ac.uk
University of Manchester https://orcid.org/0000-0002-7611-0201

Article

Keywords:

Posted Date: May 30th, 2023

DOI: https://doi.org/10.21203/rs.3.rs-2960526/v1

License: This work is licensed under a Creative Commons Attribution 4.0 International License.
Read Full License

Additional Declarations: There is **NO** Competing Interest.

Version of Record: A version of this preprint was published at Nature Communications on June 11th, 2024. See the published version at https://doi.org/10.1038/s41467-024-48592-8.

Abstract

More than 10 million people suffer from lung diseases caused by the pathogenic fungus *Aspergillus fumigatus*. The azole class of antifungals represent first line therapeutics for most of these infections however resistance is rising. Identification of novel antifungal targets that, when inhibited, synergise with the azoles will aid the development of agents that can improve therapeutic outcomes and supress the emergence of resistance. As part of the *A. fumigatus* genome-wide knockout program (COFUN), we have completed the generation of a library that consists of 120 genetically barcoded null mutants in genes that encode the protein kinase cohort of *A. fumigatus*. We have employed a competitive fitness profiling approach (Bar-Seq), to identify targets which when deleted result in hypersensitivity to the azoles and fitness defects in a murine host. The most promising candidate from our screen is a previously uncharacterised DYRK kinase orthologous to Yak1 of *Candida albicans*, a TOR signalling pathway kinase involved in modulation of stress responsive transcriptional regulators. Here we show that the orthologue YakA has been repurposed *in A. fumigatus* to regulate blocking of the septal pore upon exposure to stress via phosphorylation of the Woronin body tethering protein Lah. Loss of YakA function reduces the ability of *A. fumigatus* to penetrate solid media and impacts growth in murine lung tissue. We also show that 1-ethoxycarbonyl-beta-carboline (1-ECBC), a compound previously shown to inhibit Yak1 in *C. albicans* prevents stress mediated septal spore blocking and synergises with the azoles to inhibit *A. fumigatus* growth.

INTRODUCTION

Over 3 billion people are thought to be infected by filamentous fungi each year [1, 2]. While the vast majority of these are relatively benign there are a significant number of more sinister infections that have high mortality rates and are exceptionally difficult to treat. By far the most prominent of these are caused by the genus *Aspergillus* and result in both chronic and invasive diseases that together account for more than 1.5 million deaths each year making them among the leading cause of infection driven mortality alongside tuberculosis and malaria [1]. The World Health Organisation has recently named *Aspergillus fumigatus*, the primary etiological agent in aspergillosis, in the critical priority group of fungal pathogens [3].

Infections caused by *Aspergillus* typically originate in the lungs of susceptible individuals following inhalation of airborne fungal spores liberated from environmental sources such as compost heaps, soil and decaying vegetation. Despite the limited nutrient resources present in the lung, *A. fumigatus* spores are able to germinate and form hyphae that, in invasive disease, penetrate through the basal lamina, alveolar epithelium and basement membrane resulting in destruction of surrounding lung tissues and vasculature [4]. There are estimated to be over 300,000 cases of invasive infections every year with mortality rates ranging from 40 to 90% depending on disease setting [1, 5, 6]. With chronic forms, infections are typically restricted to cavities that have been formed by previous damage, however over time these cavities can expand and limited invasion into surrounding tissue may occur [7]. Around

3 million people are thought to have a chronic form of the disease at any one time with around 5% succumbing to infection each year [1, 7].

Our ability to treat these infections is hampered by a limited arsenal of effective antifungals [8, 9]. The triazole class are currently used as first line therapy for all forms of aspergillosis, however resistance develops frequently in chronic disease where treatments are given for a minimum of six months and are often extend well beyond this period [10, 11]. The use of compounds analogous to the azoles for crop protection has also driven resistance in the environment which has resulted in significant increases in resistance in the clinic [12]. In some centres, resistance rates in invasive aspergillosis patients who have no prior antifungal treatment now exceed 20% and these patients are more likely succumb to infection even if alternate therapies are given [13]. The rapid emergence of azole resistance in the environment and during therapy has naturally driven the use of alternative therapies however these are either poorly tolerated, in the case of amphotericin B, or are perceived to be less effective and are not orally bioavailable [14]. Combination therapy as primary treatment may prove to be more effective in supressing resistance however this is untested and the aforementioned limitations of alternative therapies restrict treatment options [15, 16]. Several novel antifungals are likely to be deployed clinically in the next few years however their development has not focussed on how and if they can be used in combination [8]. Notably we have recently shown that the activity of the novel clinical antifungal olorofim is antagonised by the azoles [17].

Here we report our efforts to identify genetic factors that facilitate adaptation of *A. fumigatus* to antifungal challenge and the mammalian host, specifically focussing on protein kinases, which are considered to be amenable for drug discovery purposes [18]. We have generated a collection of 108 genetically barcoded protein kinase null mutants in *A. fumigatus* and, using Bar-seq mediated competitive fitness profiling reveal a critical role for the dual-specificity tyrosine-regulated kinase (DYRK) YakA in adaptation to iron limitation, temperature, pH, hypoxia and azole drug stress and in contrast to the role played by its orthologue in yeast-type fungi, pathogenicity in a murine model of infection. Our data shows that, distinct from its function in yeasts, YakA has a non-redundant role in regulating adaptation to these environments by phosphorylation of proteins that control the plugging of fungal septa or cross-walls that allow compartmentalisation of hyphae. In addition to the inability to adequately adapt to micronutrient and drug stress, the lack of YakA mediated compartmentalisation of hyphal filaments prevents *A. fumigatus* from building sufficient turgor pressure to facilitate penetration into solid substrates. Finally, we show how a beta-carboline DYRK inhibitor can selectively inhibit the action of YakA to prevent septal plugging, penetration and potentiate the action of other antifungals in *A. fumigatus*.

Materials & Methods

In silico identification of kinases

Protein kinases from ORF translations for the Af293 genome were identified using Kinomer v1.0 [19, 20]. In Kinomer, a probability threshold of 0.001 was set to define a hit from this screening activity however all hits below this threshold were also evaluated using the Simple Modular Architecture Research Tool (SMART) to identify any protein kinase domains. A semantic text search to identify other previously annotated protein kinases in the genome of Af293 was performed using the term kinase at FungiDB [21]. Assessing the PFAM descriptors filtered out small molecule kinases and kinase interacting proteins [22]. PFAM domains PF02518, PF13598, PF07730 and PF07536 in the A1163 and Af293 genomes were used to identify histidine kinases. Kinases protein sequences were aligned using RaxML with default settings, and the resulting phylogenetic tree was viewed using Interactive Tree of Life (iToL) [23, 24].

Generation and validation of the A. fumigatus kinase knockout library

A. fumigatus MFIG001 was used as the parental isolate to generate kinase knockout mutants [20]. Knockout cassettes were generated using the protocol from Zhao et al 2019 [25]. Briefly, 1kb flanking regions of the gene of interest were PCR amplified and fused to a hygromycin resistance cassette via additional fusion PCR. *A. fumigatus* MFIG001 was cultured in Sabouraud agar (Oxoid, UK) overnight at 37 ºCelsius at 120 rpm, followed by protoplasting for 3 hours in Sabouraud agar + VinoTaste Pro solution (freshly filtered in 0.6M KCl, Citric Acid). Protoplasts were filtered through Miracloth, washed twice in 0.6M KCl and resuspended in 0.6 M KCl + 200 mM CaCl2. Fusion PCR product was added to $1x10^5$ protoplasts, followed by addition of PEG. This was incubated on ice for 30 minutes. 600 µL of PEG was added and the mixture was then incubated at room temperature for 10 minutes. Transformation mixture was plated on selective medium (YPS + 100 mg/L hygromycin). Transformants were twice purified on Sabouraud agar + 100 mg/L hygromycin and PCR validated.

Essential kinases

Kinase knockout mutants that could not be generated after three transformation attempts, were considered potentially essential. Repair template was generated by PCR, using the tetOFF pSK606 [26] as template and primers (Supplemental Data 1) for mutants. This repair template and crRNAs (Supplemental Data 1) were used for CRISPR-Cas9 transformations to perform promoter replacement [27]. Briefly, crRNAs were designed to target the translational start site (ATG) of each individual gene. The closest PAM site with scores above 0.5, as calculated by EuPaGDT, was used, and 20bp crRNA were ordered from Integrated DNA Technologies, UK. CRISPR/Cas9 mediated transformation was carried out as previously described. Briefly, *A. fumigatus* was grown overnight at 37 ºCelsius in Sabouraud agar, followed by protoplasting using Vinotaste. Protoplasts were washed twice in 0.6 M KCl, followed by resuspension in 0.6 KCl + 200 mM CaCl2. Guide RNA was formed by annealing crRNA to tracrRNA (IDT) and RNPs were formed by incubating at room temperature for 5 minutes with purified SpCas9 (IDT). Repair template was generated by performing PCR with 50-bp microhomology arms included in the oligos (Supplemental Data 1). Repair template, RNPs and protoplasts were mixed with PEG-$CaCl_2$, and incubated at 50 minutes on ice. 600 µL of PEG-CaCl2 was added, followed by incubation at room temperature for 20 minutes. Protoplasts were spread onto AMM + 1% Sorbitol + 100 mg/L pyrithiamine,

left at room temperature for 1 day, followed by incubation at 37 ºCelsius for 5 days. Transformants were purified twice on AMM + 100 mg/L pyrithiamine and validated by PCR.

Bar-seq

Unless otherwise stated, *A. fumigatus* strains used in this study were cultured on Sabouraud Dextrose agar (Oxoid) for 3 days at 37°C. Conidia were harvested in phosphate buffered saline + 0.01% Tween-20 (PBS-T) and collected by filtration through Miracloth (Millipore Limited cat. no. 475855). Conidia were quantified using a Fuchs-Rosenthal haemocytometer.

Conidia from each mutant was harvested and quantified using a haemocytometer, then normalised to 5 x 10^8 cell/mL and pooled into one tube. For *in vitro* competitive fitness assay, 100 µL of the pool of kinase mutants was added to each flask containing 50 mL of fungal RPMI (fRPMI) media [28] to achieve a final conidial concentration of 1 x 10^6 cells/mL. The experimental conditions included oxidative stress (1.5 mM H_2O_2), pH stress (pH4 and pH8), temperature stress (48°C and 30°C), antifungal stress (itraconazole 0.02 mg/L, voriconazole 0.15 mg/L, olorofim 0.002 mg/L) and different iron concentrations (Fe-, BPS, 30 µM, 300 µM, 5 mM). All conditions were performed in triplicate and incubated in a shaking incubator at 180 rpm for 20h at 37°C, apart from the high (48°C) and low temperature (30°C) conditions.

After incubation, the flasks were removed from the incubator and the biomass from each flask was collected using Miracloth® and a Büchner funnel under vacuum. Liquid nitrogen was used to snap freeze the dried biomass and ground into a powder, using a sterile mortar and pestle. 0.1g from each baffled flask was collected for DNA extraction.

Total fungal DNA was extracted using a standardised CTAB DNA extraction [29], for tissue samples an additional phenol:chloroform cycle was carried out. Enrichment PCR was performed using Phusion U polymerase and enrichment primers (Supplemental Data 1) for 1 cycle at 98 ºC for 30 seconds, followed by 30 cycles at 98 ºC for 10 seconds, 65 ºC for 30 seconds, 72 ºC for 30 seconds, followed by a final extension step at 72 ºC for 10 minutes. Enriched barcodes were cleaned using AMPure Beads and indexed with the Nextera XT kit (NEB) following manufacturers protocol. Indexed products were cleaned using AMPure Beads at a 1:1 ratio. Sequencing was performed on Illumina iSeq following manufacturers protocol.

Quality control of raw reads was performed using FastQC, and trimmed using CutAdapt. Trimmed reads were aligned to a Fasta file containing individual barcodes using Bowtie2. Counts per strain were obtained using BED IdXstats. Counts were normalised to total reads per sample, followed by normalisation to the input control (T0), resulting in fitness indices. Clustering was performed using Pheatmap in Rstudio with standard parameters.

Phenotypic analysis

10^3 spores of MFIG001, Δ*yakA* and Δ*yakA*::*yakA*$^+$ strains were inoculated onto solid iron deficient minimal medium (MM) [1% (w/v) glucose, Ammonium Tartrate 5 mM, $MgSO_4$ 4.3mM, KCl 7 mM, KH_2PO_4 11 mM, trace elements without iron, pH 6.5] plates with increasing concentrations of agarose (0.5 to 6%) and $FeSO_4$ (0 to 300 μM). Trace elements composition was as described in Käfer E, 1977 [30]. Plates were incubated for 48 h or 72 h at 37°C and measurements or images were taken.

Glucose uptake

10^7 spores of MFIG001, Δ*yakA* and Δ*yakA*::*yakA*$^+$ strains were inoculated in liquid complete media (CM) [2% (w/v) glucose, 0.5% yeast extract, trace elements] and incubated at 37°C and 200 rpm during 20 h. Then, all mycelia were transferred to flasks containing 50 mL of fresh liquid MM and incubated under the same conditions for additional 10 h. 100 μL aliquots were taken at 0, 4, 6, 8 and 10 h and glucose consumption was monitored by using the Glucose (GO) Assay Kit (Sigma-Aldrich), following manufacturer's instructions. The experiment was performed using biological triplicates.

Galleria mellonella and murine infection models

The *Galleria mellonella* infection model was performed as described in Johns et al 2017 [31]. Briefly larval *G. mellonella* (Live Foods Company (Sheffield, England)) (Minimum weight 0.3g; 10 per group) were inoculated by injecting 10 μL of a 1×10^6 spores/mL suspension into the last, left proleg. Sham infections were performed with PBS. Larvae were monitored daily for 8 days and scored for mortality.

The murine infection experiments were performed under UK Home office Project Licence PDF8402B7 and approved by the University of Manchester Ethics Committee. *A. fumigatus* strains were cultured on ACM containing 5 mM ammonium tartrate for 6 days at 37°C, and conidia were harvested in sterile saline and used for infection experiments. SH-*aft4* was included to allow to control for the potential effect of introducing a hygromycin selection marker [32]. CD1 male mice (19-27g) (Charles River UK, Ltd.) were housed in groups of 3–4 in IVC cages with access to food and water ad libitum. All mice were given 2 g/L neomycin sulphate in their drinking water throughout the course of the study. For the leukopenic model of infection, mice were rendered leukopenic by administration of cyclophosphamide (150 mg/kg of body weight; intraperitoneal) on days − 3, −1, + 2 and a single subcutaneous dose of triamcinolone (40 mg/kg) was administrated on day − 1. Mice were anaesthetised by exposure to 2–3% inhalational isoflurane and challenged by intranasally with a conidial suspension of 1.25×10^7 conidia/mL in 40 μL of saline solution. Mice were weighed every 24 h from day − 3, relative to the day of infection, and visual inspections were made twice daily. In the majority of cases, the endpoint for survival in experimentation was a 20% reduction in body weight measured from day of infection, at which point mice were culled. Kaplan–Meier survival analysis was used to create a population survival curve and to estimate survival over time, and *p*-values were calculated through a log rank analysis.

Histology analysis

Immunosuppressed male CD1 mice ($n = 3$) were infected as described above. After 36 h of infection, mice were culled. Lungs for histological analysis were immediately fixed in 4.0% (v/v) paraformaldehyde

(Sigma-Aldrich), and subsequently embedded in paraffin. Four-micrometer sections were stained with haematoxylin–eosin (H&E) and Grocott's Methenamine Silver (G.M.S). Images were taken using a Pannoramic 250 Flash Slide Scanner (3D HISTECH) using brightfield illumination. Analysis was performed in ImageJ.

Phosphoproteomics

Strain MFIG001 and Δ*yakA* were cultivated in AMM with iron-free Hutner's trace element solution under -Fe conditions or under + Fe conditions (addition of 30 µM $FeSO_4$) in 500 ml flasks for 18 h, 200 rpm at 37°C. Mycelia were harvested using Miracloth (Merck Millipore, Germany) and disrupted by using mortar and pestle with liquid nitrogen. Cell debris were homogenized in lysis buffer (1% (w/v) SDS, 150 mM NaCl, 100 mM TEAB (triethyl ammonium bicarbonate), one tablet each of cOmplete Ultra Protease Inhibitor Cocktail and PhosSTOP). After addition of 0.5 µL Benzonase nuclease (250 U/µL) the samples were incubated at 37°C in a water bath sonicator for 30 min. Proteins were separated from unsolubilised debris by centrifugation (15 min, 18000 x *g*). Each 6 mg of total protein per sample was diluted with 100 mM TEAB to gain a final volume of 4 mL. Subsequently, cysteine thiols were reduced and carbamidomethylated in one step for 30 min at 70°C by addition of 120 µL of 500 mM TCEP (tris(2-carboxyethyl)phosphine) and 120 µL of 625 mM 2-chloroacetamide (CAA). The samples were further cleaned up by precipitation with 20% trichloroacetic acid (TCA) for 30 min on ice. After centrifugation (20 min at 20000 *g*), the precipitate was washed with 90% acetone. Protein precipitates were resolubilized in 5% trifluoroethanol of aqueous 100 mM TEAB and digested overnight (18 h) with a Trypsin + LysC mixture (Promega) at a protein to protease ratio of 25:1. An aliquot of 0.2 mg digested protein was used for the reference proteome analysis and 5.8 mg was used for the phosphopeptide enrichment. Samples were evaporated in a SpeedVac. The reference proteome sample was resolubilized in 50 µL of 0.05% TFA in H2O/ACN 98/2 (v/v) filtered through PES 10kDa MWCO membrane spin filters (VWR). The filtrate was transferred to HPLC vials and injected into the LC-MS/MS instrument.

Phosphopeptides were enriched by using TiO_2 + ZrO_2 TopTips (Glygen Corp., Columbia, MD, USA). TopTips were loaded with 500 µg protein isolate using 12 TopTips per biological replicate after equilibration with 200 µl Load and Wash Solution 1, LWS1 (1% trifluoroacetic acid (TFA), 20% lactic acid, 25% acetonitrile (ACN), 54% H2O). TopTips were centrifuged at 1500 rpm (~ 200 x *g*) for 5 min at room temperature. After washing with 200 µL LWS1, the TiO_2/ZrO_2 resin was washed with 25% ACN and subsequently the phosphopeptides were eluted with 200 µL $NH_3 \cdot H_2O$ (NH_4OH), pH 12. The alkaline solution was immediately evaporated using a SpeedVac. The phosphoproteome samples were resolubilized in 50 µL of 0.05% TFA in H_2O/ACN 98/2 (v/v) filtered through PES 10 kDa MWCO membrane spin filters (VWR). The filtrate was also transferred to HPLC vials and injected into the LC-MS/MS instrument.

Each sample was measured in triplicate (3 analytical replicates of 3 biological replicates of a reference proteome fraction and a phosphoproteome fraction. LC-MS/MS analysis was performed on an Ultimate 3000 nano RSLC system connected to a QExactive HF mass spectrometer (both Thermo Fisher

Scientific, Waltham, MA, USA). Peptide trapping for 5 min on an Acclaim Pep Map 100 column (2 cm x 75 µm, 3 µm) at 5 µL/min was followed by separation on an analytical Acclaim Pep Map RSLC nano column (50 cm x 75 µm, 2µm). Mobile phase gradient elution of eluent A (0.1% (v/v) formic acid in water) mixed with eluent B (0.1% (v/v) formic acid in 90/10 acetonitrile/water) was performed using the following gradient for the more hydrophilic phosphoproteome samples: 0–5 min at 4% B, 15 min at 7% B, 50 min at 10% B, 100 min at 14% B, 150 min at 25% B, 190 min at 60% B, 205–215 min at 96% B, 215.1–240 min at 4% B. The reference proteome gradient was as follows: 0–4 min at 4% B, 10 min at 7% B, 50 min at 12% B, 100 min at 16% B, 150 min at 25% B, 175 min at 35% B, 200 min at 60%B, 210–215 min at 96% B, 215.1–240 min at 4% B.

Positively charged ions were generated at spray voltage of 2.2 kV using a stainless steel emitter attached to the Nanospray Flex Ion Source (Thermo Fisher Scientific). The quadrupole/orbitrap instrument was operated in Full MS / data-dependent MS2 Top15 mode. Precursor ions were monitored at m/z 300–1500 at a resolution of 120,000 FWHM (full width at half maximum) using a maximum injection time (ITmax) of 120 ms and an AGC (automatic gain control) target of $3x10^6$. Precursor ions with a charge state of z = 2–5 were filtered at an isolation width of *m/z* 1.6 amu for further HCD fragmentation at 27% normalized collision energy (NCE). MS2 ions were scanned at 15,000 FWHM (ITmax = 100 ms, AGC = $2x10^5$) using a fixed first mass of *m/z* 120 amu. Dynamic exclusion of precursor ions was set to 30 s and the minimum AGC target for Precursor ions selected for HCD fragmentation was set to $1x10^3$. The LC-MS/MS instrument was controlled by Chromeleon 7.2, QExactive HF Tune 2.8 and Xcalibur 4.0 software.

Tandem mass spectra were searched against the FungiDB database (2021/10/26 (YYYY/MM/DD); https://fungidb.org/common/downloads/Current_Release/AfumigatusAf293/fasta/data/FungiDB-54_AfumigatusAf293_AnnotatedProteins.fasta) of *Aspergillus fumigatus* Af293 using Proteome Discoverer (PD) 2.4 (Thermo) and the algorithms of Mascot 2.4.1 (Matrix Science, UK), Sequest HT (version of PD2.4), MS Amanda 2.0, and MS Fragger 3.2. Two missed cleavages were allowed for the tryptic digestion. The precursor mass tolerance was set to 10 ppm and the fragment mass tolerance was set to 0.02 Da. Modifications were defined as dynamic Met oxidation, phosphorylation of Ser, Thr, and Tyr, protein N-term acetylation and/or loss of methionine, as well as static Cys carbamidomethylation. A strict false discovery rate (FDR) < 1% (peptide and protein level) and a search engine score of > 30 (Mascot), > 4 (Sequest HT), > 300 (MS Amanda) or > 8 (MS Fragger) were required for positive protein hits. The Percolator node of PD2.4 and a reverse decoy database was used for qvalue validation of spectral matches. Only rank 1 proteins and peptides of the top scored proteins were counted. Label-free protein quantification was based on the Minora algorithm of PD2.4 using the precursor abundance based on intensity and a signal-to-noise ratio > 5. Normalization was performed by using the total peptide amount method. Imputation of missing quan values was applied by using abundance values of 75% of the lowest abundance identified per sample. For the reference proteome analysis used for master protein abundance correction of the phosphoproteome data, phosphopeptides were excluded from quantification. Differential protein abundance was defined as a fold change of > 2, p-

value/lABS(log4ratio, < 0.05 and at least identified in 2 of 3 replicates. Differential phosphopeptide abundance was defined as a fold change of > 2, ratio-adjusted pvalue < 0.05 pvalue/ABS(log4ratio) and at least identified in 2 of 3 replicates.

Microscopic analysis

The LahC:GFP and HexA:GFP were obtained from Frank Ebel [33, 34]. For live-cell imaging in liquid cultures, conidia at concentration of 5×10^5 cells/mL were dispensed into the wells of an 8-well ibidi imaging chamber (ibidi GmbH, Martinsried, Germany), and incubated in 250 µL Hutner's minimum media (HMM) for 20 h at 37°C for the development of matured hyphae before imaging. The imaging chamber was filled with medium (either iron depleted or replete HMM) dependent on the needs of each individual experiment. For medium shifting experiments, 250 µL of the extant culture medium was removed from each well of the imaging chamber and replaced with desired medium (either iron repleted HMM, iron depleted HMM or iron depleted HMM with different reagents) by pipetting. Reagents used to supplement medium included rapamycin (10 µM), H_2O_2 (3 mM), caspofungin (0.03 mg/L), voriconazole (1.5 mg/L) or 1-ECBC (500 µM) or 1.8 M glycerol. Fungal cells were imaged for periods of up to 1 h at 37°C in a temperature-controlled chamber mounted on the microscope stage.

For live-cell imaging of fungal penetration on solid medium, 100 conidia were spotted on the surface of HMM media containing 3% or 4% of agarose. The petri dishes containing inoculated media were wrapped in Parafilm and incubated at 37°C for 24 h. Before imaging, a cubic of the media (approximately 1 cm x 1 cm) with the fungal colony in the centre was cut out using a sterile scalpel, and placed into a well of an imaging chamber facing downwards. The well was prefilled with 100 µL of distilled water.

Live-cell imaging of *A. fumigatus* in liquid cultures was performed using a Leica TCS SP8 confocal laser-scanning microscope (Leica Microsystems Ltd., Milton Keynes, UK) equipped with photomultiplier tubes, hybrid GaAsP detectors and a 63x water immersion objective. Excitation and emission wavelength of 496 nm and 515–545 nm respectively were used for imaging the GFP expressed by *A. fumigatus*.

For live-cell imaging of fungal penetration on solid medium, a long working distance 25x water immersion objective lens was employed instead. The 'Z-compensation function' was used for fine adjustment of the laser excitation to compensate the signal reduction in the deeper section of the solid media. These adjustments were done across 3 points of the z-stack, preventing over or under-exposure of acquisition. Acquired images were analysed using Imaris v8.0 software (Bitplane Scientific software module; Zurich, Switzerland).

In silico **small molecule screening**

The structure of YakA kinase domain (Y345-I676), as predicted by ScanProsite [35], was determined using AlphaFold2 [36], for subsequent analysis, the highest-scoring model was used (pLDDT: 96.1, pTMscore: 0.9375). VSpipe [37], a semi-automated pipeline, was used for blind docking with the Maybridge Ro3 1000 fragment library using AutoDock Vina [38]. This library contains 1000 chemically

diverse, rule of three (Ro3) compliant, and pharmacophore-rich fragments. Clusters were defined as having at least 15 fragments bind to it. 1-ECBC was also used for docking using AutoDock Vina. Druggable pockets were predicted using PockDrug [39], an online server which assess pocket geometry, hydrophobicity, and aromaticity and gives a druggability score where scores of > 0.5 are considered druggable. Outputs from all programmes were visualised in PyMOL 2.5.

Data availability statement

Mass spectrometry proteomics data are available from the ProteomeXchange Consortium via the PRIDE partner repository [xy] with dataset identifier XYZ.

Results

Annotation of the protein kinases of A. fumigatus **and generation of a barcoded null mutant library.**

The protein kinase (PK) complement in *A. fumigatus* has been defined either from homology to annotated proteins in *Aspergillus nidulans* [40] or bespoke assessment of now defunct annotations of the *A. fumigatus* genome using Hidden Markoff Models (HMM) [41]. We therefore performed a *de novo* evaluation of a recently updated annotation of the *A. fumigatus* (Af293) genome using the HMMer and the kinomer HMM Library [42] to identify novel protein kinases. The hits from this library were supplemented with PKs identified via semantic searches of the annotated genome databases at AspGD and FungiDB. A total of 133 unique PKs were identified using kinomer with an additional 19 (all of which were histidine kinases) being found through database searches (Supplementary Table 1). An assessment of the genome of another sequenced strain of *A. fumigatus*, A1163 revealed the presence of 155 protein kinases. Pairwise comparison of the two PK cohorts revealed that 2 of the protein kinases identified in Af293, did not have an annotated orthologue in A1163 (Afu7g04735, Afu1g16000). Interestingly, comparison of mapped RNAseq data to the A1163 genome indicates that Afu7g04735 has been misannotated in Af293 [43]. When corrected, Afu7g04735, Afu1g16000 share (98%) sequence identity and may be the result of a recent gene duplication event. BLASTn analysis of the A1163 genome with the Afu1g16000 and Afu7g04735 coding sequence revealed regions sharing 95% and 100% sequence identity respectively indicating missing annotations from this genome. Similarly, 8 protein kinases from A1163 did not have reciprocal BLAST hits in Af293. Of these, 2 (AFUB_079830 and AFUB_071620) seemed to be duplications of another protein kinase (AFUB_044560; Afu3g03740), 3 had regions of the genome that share > 90% sequence identity with Af293 however the ORFs appear to have been truncated while 3 were missing altogether from the Af293 genome.

The disparity in the conservation of the PK cohort between the 2 strains led us to assess if these proteins were conserved across 218 *A. fumigatus* sequenced isolates [12]. Of the 155 protein kinases in A1163, 137 were considered core (i.e. found in all genomes) while 22 kinases were considered accessory genes. BLASTP analysis of all of the protein kinases from Af293 was performed against databases from all mammalian species in an attempt to identify those kinases that have the potential to

be fungal specific drug targets, i.e those showing little similarity with mammalian kinases. Nineteen protein kinases were identified that were either absent in all mammalian species (no detectable BLAST hit) or shared very little sequence identity (e value > $1x10^{-10}$; Supplemental Data 1). In an attempt to assess the evolutionary lineage of the non-mammalian kinases, a phylogenetic tree was built (Fig. 1A). Consistent with our classification data from Kinomer, the vast majority of the kinases that fall into specific kinase categories clustered together. Two clear evolutionarily distinct clusters were identified, encapsulating kinases Afu3g13210, Afu3g08710, Afu6g03252, Afu5g15080 (Cluster FF1) and Afu1g16060, Afu5g14970, Afu3g02740 Afu6g03240. All of these protein kinases are conserved in A1163.

To construct a null mutant library of the PKs we had identified, we chose to employ a fusion PCR approach described by Zhao et al and previously used to generate a 484-member library of transcription factor null mutants [25, 43]. A unique 20-bp barcode sequence flanked by universal regions was introduced at the time of strain disruption to enable assessment of fitness in pooled assays using bar-seq. Cassettes were successfully amplified for 160 kinase genes, and were used to transform MFIG001, a *Δku80*, *pyrG+* strain derived from FGSC strain A1160 [20]. We isolated homokaryotic null mutants for 108 (67.5%) protein kinase genes (Fig. 1A) but despite several attempts (minimum $n = 3$), we were unable to isolate null mutants for 52 kinases (Supplementary Table 1). Of the protein kinase genes that we were unable to generate a homokaryotic null mutant for, all were considered core kinases. Our inability to isolate homokaryotic null mutants is indicative of gene essentiality. To verify this, strains carrying tetracycline repressible alleles were generated for 4 of the genes in our list, all of which lacked growth in the presence of doxycycline (Fig. 1B). For 18 of these genes, gene disruption mutants have previously been obtained by using a CRISPR-Cas9 mediated knock-in approach [44].

High throughput competitive fitness reveals protein kinases required for A. fumigatus adaptation to stress and virulence.

The introduction of unique genetic barcodes in our *A. fumigatus* null mutant collection enabled us to perform competition experiments between strains. Using procedures that limit hyphal fusion and nuclear exchange between strains [45] we carried out *in vitro* competitions in 12 different growth conditions that induce micronutrient (iron), temperature, pH, antifungal and oxidative stress (Fig. 2A). Hierarchical clustering of this quantitative pheno-profiling data revealed functionally supported links between MAP kinases with known regulatory connectivity. Specifically, the cell wall integrity signalling cascade, which is comprised of *mpkA* (AFUB_070630), *mkk2* (AFUB_006190) herein named *mkkA* to conform to *A. fumigatus* gene nomenclature standards and *bck1* (*bckA*; AFUB_038060), form a compact cluster by virtue of their reduced ability to adapt to changes in pH and temperature [46]. Interestingly, the phenotypes exhibited by the *bckA* null mutant were significantly less pronounced than that of the downstream targets of the cascade when placed under iron stress. This is consistent with previous reports that the phenotype of a *bckA* disruptant is less severe [44], and indicates a level of redundancy or functional divergence at the start of this signalling module. The two other well defined MAP kinase signalling cascades (High osmolarity and pheromone response pathways) failed to cluster either

because members were missing from the null mutant collection (*mpkB* and *pbsB*) or we did not screen under conditions likely to exhibit a strong phenotype. Interestingly novel functional clusters were identified including *halA* (AFUB_053500), an orthologue of the *S. cerevisiae* salt tolerance kinase HAL4 and *skyA* (AFUB_096590). Both have growth defects in the high salt containing Aspergillus Minimal Media (AMM) and a competitive advantage in low iron environments however the Δ*skyA* alone has a distinct defect in adaptation to high temperature.

The barcoded collection also afforded the opportunity to quantitatively assess competitive fitness of isolates within a murine model of infection. Of the strains assessed, 3 protein kinase mutants had a demonstrable and statistically supported reduced fungal burden in mice with chemically induced leukopenia, namely Δ*pkaC* (AFUB_027890;) which had a mean log2 fold change in normalised barcode counts of -9.7, Δ*mpkA* (-14.3 Log2FC) and Δ*mkkA* (-12.8 Log2FC) [47]. A further 9, Δ*bckA* (ΔAFUB_038060), Δ*rfeA* (AFUB_090090), Δ*scy1* (ΔAFUB_063270), ΔAFUB_075230, Δ*chkb* (ΔAFUB_089280), Δ*nnk1* (ΔAFUB_011380), Δ*halA* (ΔAFUB_053500), ΔAFUB_044400, and ΔAFUB_099170 (an orthologue of the *yak1* protein kinase of *S. cerevisiae* and herein defined as *yakA*) had notable (<-1.4 Log2FC) reductions of relative fungal burden however they failed to reach statistical significance in this experiment (**Supplemental Data 2, Supplemental Fig. 1**). Crucially however we were able replicate and statistically verify the modest defect in virulence we observed in the murine competition infection model for the *yakA* null mutant in a *Galleria mellonella* model of aspergillosis and a leukopenic murine model of aspergillosis when they were challenged with single isolates (Fig. 2D **and E**). The indicative loss of fitness of the *yakA* mutant in the murine lung, an environment known to be micronutrient limited, correlated with a significant reduction in fitness in low iron environments (-1.15 log2FC in 0 mM Fe AMM, -2.96 log2FC when BPS was added as chelator) but not under control growth conditions (RPMI-1640; 37 Celsius pH 7.0). The *yakA* mutant was of further interest as it also exhibited a striking reduction in competitive fitness when placed under azole stress (-4.6 log2FC; padj $3.99x10^{-34}$) marking it as a potential target for the development of a novel antifungal that could both treat infection and work synergistically with the azole class of antifungals that represent the current gold standard treatments for all forms of aspergillosis.

Comparative phenotyping was performed to assess the extent of the defects observed in the Δ*yakA* mutant. Biomass was reduced by 89% when compared to the wild-type isolate upon exposure to 0.5 mg/L of itraconazole while the MIC was reduced by 2-fold (Fig. 2B). In solid media, growth of the *yakA* mutant was significantly impaired in low iron and zinc environments and was notably reduced under high pH stress, consistent with the reduced solubility of both iron and zinc in alkaline environments (Fig. 2C). Interestingly, and contrary to our expectations, Δ*yakA* did not show any discernible growth defect under iron limitation in static liquid medium (**Supplemental Fig. 2**). These findings led us to characterise the function of YakA in more detail.

YakA is required to facilitate penetration and establish turgor pressure.

YakA is a DYRK kinase, which has been described in several other fungi including *C. albicans*, *S. cerevisiae*, *Fusarium* species, *Penicillium* species, *Magnaporthe oryzae* and *Botrytis cinerea* [48–52] and been shown to function by phosphorylating transcription factors in response to stress. Specifically in *S. cerevisiae*, the orthologue *yak1* is under control of the Tor kinase and is imported into the nucleus in response to various stressors which initiates the activation of the transcriptional regulators Haa1, Pop3, Hsf1, Msn2 [53]. Notably it has been suggested that in *Fusarium graminearum* YakA phosphorylates HapX, a transcription factor responsible for regulating iron homeostasis in filamentous fungi [54].

Alignment of YakA orthologues indicate that the protein encoded in *A. fumigatus* is larger than of the *C. albicans* Yak1 (894 AA and 809 AA, respectively) (**Supplemental Fig. 3**). While the protein kinase domain is well conserved (51% ID), the C- and N-terminal domains of the *A. fumigatus* protein lack similarity to their yeast counterparts. This led us to hypothesise that the *A. fumigatus* YakA may have different or additional functions to the *C. albicans* Yak1.

Consistent with the role of Yak1 in sensing carbon starvation, Δ*yakA* was unable to effectively utilise xylose and fructose and had severe growth defects in the non-fermentable carbon source glycerol, acetate and ethanol (**Supplemental Fig. 4**). However, when grown in the presence of combinations of glucose and xylose we saw no evidence that the *yakA* mutant was unable to switch between using different carbon sources indicating that the function of YakA in *A. fumigatus* differed from that of Yak1 in yeasts. Furthermore, and inconsistent with a role for YakA in generalised activation of HapX, Δ*yakA* had no defect in iron chelating siderophore production in low iron environments (**Supplemental Fig. 2B**)

Interestingly, the stress induced growth defects we observed in the *yakA* mutant was more profound when we increased the agarose concentration of solid medium (Fig. 3A). Three-dimensional tracking of fungal hyphae growing into the solid medium showed that Δ*yakA* was able to penetrate through the media at 3% agarose, but not at 4% (**Supplemental Fig. 5A**). This phenotype was exacerbated under iron limitation (**Supplemental Fig. 5B**). This led us to investigate if the inability of the Δ*yakA* mutant to penetrate the mammalian lung during infection was linked to the reduction in virulence. Cross sections of infected lung tissue revealed large lesions in wild-type and the genetically reconstituted mutant strain with hyphae appearing throughout the lung (Fig. 3B). However, for the *yakA* mutant, only small lesions were evident in infected lungs, and consistent with our hypothesis, limited penetration of the squamous epithelial layer into the surrounding lung tissue was observed (Fig. 3C). Interestingly we identified limited instances of airway plugging caused by the *yakA* mutant growing within alveoli (**Supplemental Fig. 5C**) indicating a likely cause of mortality in mice infected with the *yakA* mutant.

To penetrate stiff substrates filamentous fungi require the build-up of significant turgor pressure within the hyphae [55]. We therefore assessed the ability of Δ*yakA* to re-establish turgor after cytorrhysis [56]. After induction of cell collapse, the wild-type isolate was able to fully recover within 8 minutes however, the Δ*yakA* membrane collapsed further and was unable to fully recover, even after 20 minutes (Fig. 3C) suggesting loss of penetrative ability could be linked to failure to establish sufficient turgor pressure.

YakA regulates phosphorylation of proteins associated with the septal pore.

There was a clear disconnect between the inability of the *yakA* null to grow effectively in low iron environments, its perceived role in the regulation of the iron homeostasis transcription factor HapX and its unaltered ability to regulate the production of siderophores. In an attempt to uncover why this could be we assessed phosphoregulatory role of *yakA* under iron limiting conditions (Fig. 4A). Overall, 18,076 phosphopeptides were detected from 2929 proteins (**Supplemental Data 3**). K-means clustering (n = 10) of differentially phosphorylated peptides under iron limitation revealed clusters of peptides that were regulated in an YakA dependent (n = 1174 downregulated – cluster 1, n = 330 upregulated - cluster 2 [Figure 4A]) and YakA independent manner (n = 557 downregulated – cluster 3, n = 434 upregulated - cluster 4**)** (Fig. 4A). Consistent with our observations that siderophore levels were unchanged in the YakA null mutant, peptides derived from siderophore and iron transporters MirB, Sit1 and Sit2 had higher levels of phosphorylation under iron deplete conditions (MirB: 399 log2 fold up, Sit1: 8.3 log2 fold up, Sit2: 4.1 log2 fold up, MirC: 5.0 log2 fold up) but were not affected by loss of YakA (cluster 4; Fig. 4A). Peptides from proteins involved in siderophore biosynthesis were also found within cluster 4 (SidT: 692 fold up, SidA: 4.8 fold up, SidD: 240 fold up, SidG 6.1 fold up, SidL: 4.55 fold up,) (Supplementary Data 2).

A GO-term analysis (cellular component) of iron regulated phosphorylation that was dependent on YakA included proteins involved in cell morphology, division, the septum, membrane and cellular homeostasis (cytoskeleton, vesicle and nuclear pore) (Fig. 4B). An association between YakA and phosphorylation of proteins associated with the septum, a cross-wall structure that divides hyphal cells and is required for the generation of turgor pressure [57, 58], could explain the penetration defect observed in the Δ*yakA* strain. A more detailed analysis of proteins known to be involved in septal formation showed that those with the biggest phosphorylation changes are essential for septal plugging (Fig. 4C). Notably, these include the leashin protein Lah which tethers a plug known as the Woronin body to the septa, a septal pore associated protein, Spa10 which stabilizes Lah at the septal pore and Soft (SO) a scaffolding protein associated with the septal pore upon cell wounding [57]. These results suggested that YakA has a critical role in regulating septal plugging under stress.

YakA localises to the septal pore and regulates septal plugging by HexA and Lah.

In order to assess the cellular localisation of YakA we generated a strain expressing a YakA-GFP fusion strain. YakA-GFP signal was detectable but dim under iron replete medium (Fig. 5A). We hypothesised that similarly to Yak1 in *S. cerevisiae*, we would observe a response when adding rapamycin, which inhibits the action of TOR, a known negative regulator of Yak1. In line with previous findings, YakA-GFP signal became brighter upon rapamycin addition however unlike in *S. cerevisiae*, YakA did not localise to the nucleus but consistent with our phosphoproteomic data localised to the centre of fungal septa at the presumptive septal pore (Fig. 5A **and B**). Furthermore, the increase in apparent abundance of YakA and septal localisation was induced by iron limitation (Fig. 5A).

Our data led us to explore the role of YakA in the localisation of the Woronin body associated protein HexA and its tether Lah (**Supplemental Fig. 6**). As expected, a C-terminally GFP tagged HexA (HexA:GFP) and the septal pore associated domain of Lah (LahC:GFP) localised to the septal pore in response to iron

limitation (Fig. 6A). Deletion of *yakA* in the LahC:GFP background resulted in complete loss of the GFP signal from the fungal septum. Deletion of *yakA* in the HexA:GFP background was not expected to prevent localisation of HexA to the septa as its peroxisomal targeting sequence is blocked by the GFP tag. However, consistent with loss of Lah function in this genetic background [33], the GFP signal became less centrally located and more widespread across the fungal septum in *yakA* null mutant (Fig. 6B). Together these data suggest that YakA activity is required for micronutrient stress-initiated localisation of Lah and HexA at the septal pore and subsequent septal plugging.

YakA can be inhibited by the action of beta-carbolines to prevent septal plugging and potentiate azole action.

We hypothesised that YakA could function as a novel antifungal target as it is required for pathogenicity and adaptation to the azole and echinocandin class of antifungals (**Supplemental Fig. 7**). We therefore explored the druggability of YakA by performing a virtual screening of small molecules against an AlphaFold predicted structure of YakA (Fig. 7A). Through blind docking, clusters of ligands binding to three pockets were identified, one in the active site and two smaller clusters within the C-lobe of the protein [37]. Of these three sites, the most probable druggable pocket was within the active site (0.81 druggability score as defined by PockDrug). This pocket consists of 30 amino acid residues with a volumetric hull of 2363.73 A. In a previous study, the Yak1 protein of *C. albicans* was shown to be inhibited by the beta-carbolines 1-ECBC and 1-ABC, the latter being a small molecule produced by *Lactobacillus* species. 1-ECBC bound with high affinity (ΔG: -7.7 kcal/mol; figure) to the active site pocket of the predicted *A. fumigatus* YakA protein [59].

To obtain evidence that YakA can be chemically inhibited, we challenged *A. fumigatus* with 1-ECBC under iron replete and limiting conditions and assessed the impact of localisation of YakA and Lah (**Supplemental Fig. 8A**, Fig. 7B). Upon iron limitation 1-ECBC blocks YakA recruitment to the septal pore, which is turn blocks LahC recruitment (Fig. 7B). Interestingly, this phenomenon was only observed when YakA was not already present at the septal pore indicating that unblocking of the septal pore is a YakA independent process (**Supplemental Fig. 8B**). As the Δ*yakA* mutant is hypersensitive to the azoles we explored the combinatorial effect of voriconazole and 1-ECBC to inhibit growth of MFIG001 (Fig. 7C). A strong synergistic effect (FICI = 0.28) was observed in a checkerboard assay.

Taken together, we have shown that generation of mutant collections for the purpose of competitive fitness profiling can be deployed to identify novel drug targets in *A. fumigatus* using both *in vitro* and *in vivo* assays. Using this strategy, we have identified YakA, a DYRK kinase, that is required for adaptation to azoles, iron homeostasis through its role as a mediator of septal plugging. We also demonstrate YakA is a druggable kinase, which can be targeted by natural products of the beta-carboline class to prevent septal plugging and potentiate the action of the azoles in *A. fumigatus*.

Discussion

A dearth of antifungal agents and pandemic of antifungal drug resistance is hampering treatments of aspergillosis [9, 60]. It is critical that strategies are developed to improve treatment outcomes and development of novel antifungal agents is a key way this objective will be achieved [9]. Here, through our assessment of the kinome of *A. fumigatus* we have shown how high throughput functional genomics can enable the detection of novel targets that co-ordinately regulate adaptation to the host environment and antifungal challenge.

Competitive fitness profiling of large knockout libraries has been used to great effect in microbes to identify hitherto unknown critical functions for genes in adaptation to numerous stressors [61, 62]. More recently these approaches have taken advantage of massively parallel sequencing technologies to assess fitness of barcoded collections in yeasts [63]. There are however difficulties with applying competitive fitness profiling to filamentous fungi as hyphae of isotype strains can anastomose (fuse), allowing exchange of genetic material between hyphae [45]. This is compounded by the fact that unlike yeasts, filamentous fungi compromise of multinucleate hyphal compartments and heterokaryons formed through this process are likely to impact the effect of an individual mutation [64–66]. In *A. fumigatus* however, hyphal fusion occurs rarely in laboratory conditions unless strains are placed under stress and then only when cultured on solid media [45, 64]. Taking advantage of this, and our ability to generate barcoded null mutants rapidly in *A. fumigatus* [25], we have developed an accessible approach to evaluate strain fitness in a collection of protein kinase null mutants. Hierarchical clustering of our data highlights the previously described interconnectivity of a number of protein kinases including the cell wall integrity (CWI) MAPK signalling pathway [46] and also reveals potential links between other regulators such as *halA* (AFUB_053500), an orthologue of the *S. cerevisiae* salt tolerance kinase HAL4 and *skyA* (AFUB_096590). While these associations do not necessarily represent direct interactions, it is possible that these kinases may regulate an overlapping cohort of proteins.

In this study we also demonstrate that competitive profiling can be applied to animal models of infection. We have shown that two protein kinases with known defects in virulence, namely *pkaC1* (AFUB_027890) [67], and the CWI signalling kinase *mkkA* (AFUB_006190) [68] have significant reductions in fitness in a leukopenic murine model of infection. Our data is equally compelling for another member of the CWI-MAPKs cascade, MpkA, which, however, showed no significant reduction in virulence in a neutropenic mouse infection model [46]. The Δ*bckA* mutant, lacking the MAP3K member of the CWI-MAPK cascade, also showed a fitness defect in the murine model, alongside several other protein kinases including Δ*yakA* (ΔAFUB_099170). However, variability within experiments resulted in these reductions in virulence not reaching statistical significance. Interestingly, the distribution of fitness values for replicates in the mouse model was bimodal, perhaps indicating that the stress caused by exposure to the murine lung could be inducing hyphal fusion which in turn would mask fitness defects in these strains [45]. Alternatively, as seen in our histological data from mice infected with the Δ*yakA* isolate, the data may indicate that growth of Δ*yakA* is discontinuously distributed throughout the various niches within the lung.

YakA is one of two DYRK kinases in *A. fumigatus*, however our data indicate that it has a non-redundant role in adaptation to pH stress, triazole stress, non-fermentable carbon sources, environments with physiological levels of iron, the ability to penetrate solid substrates and establish an infection in a murine model of aspergillosis. In *S. cerevisiae*, the YakA orthologue, Yak1p is a core component of the glucose sensing system that is negatively regulated by TOR [69]. Upon activation, Yak1p is imported into the nucleus where it phosphorylates a suite of transcription factors including Pop2p, Msn2, Msn4 and Hsf1p which in turn initiate transcriptional adaptive stress responses [53, 70]. Recently it has been suggested that Yak1 is localised to the nucleus and directly phosphorylates the iron homeostasis transcription factor HapX to facilitate adaptation to high iron levels in the filamentous fungus *Fusarium graminarum* [54]. Although our phosphoproteomic data indicates that HapX is phosphorylated (position 370–383), we saw no evidence that this was in response to YakA activity nor did we see any evidence of nuclear localisation of YakA in response to iron depletion, rather our data indicates that upon stress YakA localises to the septal pore. Consistent with this, we were unable to show a role for YakA in direct regulation of biosynthesis of the siderophore TAFC. Furthermore, although the phosphoproteomic profiles we observed revealed a key role for YakA in regulating 28% of the phosphopeptides observed in response to iron depletion, critically it was not involved in regulating the phosphorylation of proteins involved in siderophore biosynthesis or iron uptake (Supplemental Data 3).

A. fumigatus hyphae are considered to be largely syncytial, i.e the content of the cytoplasm is near-uniformly distributed and readily exchangeable. However, the hyphae of filamentous fungi have cross walls, termed septa, that enable compartmentalisation of cellular material [71]. These septa have pores that permit streaming of cytoplasm and between compartments but these pores can be transiently blocked by an organelle known as the Woronin body [72]. It has been postulated that septal pore blocking permits an effective way of transiently controlling protein, nucleic acid and nutrient concentrations between compartments [73]. Notably, the phosphopeptides dysregulated upon loss of *yakA* were heavily enriched from proteins associated with the septa. This aligned with our data that shows YakA localising to the septal pore in response to low iron stress. We also show that septal plugging by the Woronin body complex component HexA, and localisation of the C-terminal domain of the leashin Lah, a protein that tethers HexA to the septa, is YakA dependent and this localisation is also triggered in low iron environments. Seemingly therefore, YakA has been repurposed in *A. fumigatus* to regulate hyphal compartmentalisation upon stress. However, like Yak1 in *S. cerevisiae*, activation of YakA can be induced by rapamycin and hence appears to be under the control of TOR complex. Intriguingly, it has been demonstrated that the TOR kinase is a key regulator of iron homeostasis, including the transcriptional regulator HapX [74]. Our current hypothesis therefore is that, under iron limitation TOR activity is reduced, resulting in a cascade that results in activation of siderophore production via HapX and initiation of septal blocking by the Woronin body, mediated by YakA to enrich the growing tip for iron.

The overall objective of this study was to identify novel targets for antifungal therapy that would enable the development of compounds that could synergise with the azoles. Serendipitously, as we were discovering the role of YakA in septal plugging, a novel inhibitor of *C. albicans* Yak1 was being described

[59]. The *Lactobacillus* derived compound 1-acyl-β-carboline (1-ABC) was shown to prevent Yak1-mediated filamentation of *Candida* species and inhibit Yak1 activity *in vitro*. Here we have shown that an analogue 1-ECBC is able to prevent low-iron induced septal plugging. Intriguingly however, once septa are blocked, chemical inhibition of YakA activity does not appear to unblock septal pores, indicating that unblocking septa either does not occur in low-iron conditions or that unblocking of septa is mediated by another, as yet unidentified protein. Consistent with our evidence, and that of others [75] that septal plugging is critical for adaptive response to triazole drug challenge, 1-ABC synergises with voriconazole to inhibit growth of *A. fumigatus*. As we have shown that YakA is also required for virulence of *A. fumigatus*, there is a clear possibility that β-carbolines, which have been developed to target the YakA orthologue DYRK1A for use as an anti-depressant or a treatment for Parkinson's disease, could represent a novel class of clinical therapeutics that synergise with the azoles [76].

YakA inhibitors may also have value in crop protection. In the cereal pathogen *Fusarium graminearum* [54], the rice blast fungus *Magnaporthe oryzae* [51] and *Botrytis cinerea* [50], the causative agent of grey mould, Yak1 orthologues have been shown to be essential for virulence and in the case of *Magnaporthe oryzae*, required for the formation of a cell essential for pathogenesis known as the appressorium. It is noteworthy that many plants produce β-carboline alkaloids and it is interesting to speculate that production of such compounds may provide a natural defence against fungal pathogens [77].

To summarise, we have applied a functional genomic approach to identify novel targets for antifungal therapy. In doing so we have uncovered a novel role for the DYRK1 kinase YakA in the regulation of septal pore plugging. Chemical perturbation of YakA function using 1-ABC enhances the action of the azole class of antifungals s opening the possibility that β-carbolines could be developed for clinical and/or agricultural purposes.

Declarations

Acknowledgements

We thank Silke Steinbach for technical support and Robb Cramer for help with discussions around the function of YakA. We would also like to thank Leah Cowen for sending us the 1-ECBC compound. This work was funded by the Deutsche Forschungsgemeinschaft (DFG, German Research Foundation) Collaborative Research Centre/Transregio FungiNet 124 'Pathogentic fungi and their human host: Networks of Interaction' (project number 210879364; project A1 and Z2) and the International Leibniz Research School (ILRS) for Microbial and Biomolecular Interactions as part of the excellence graduate school Jena School for Microbial Communication (JSMC). We thank Fundação de Amparo à Pesquisa do Estado de São Paulo (FAPESP) 2021/04977-5 (GHG) and 2020/01131-5 and 2018/00715-3 (CV) and Conselho Nacional de Desenvolvimento Científico e Tecnológico (CNPq) 301058/2019-9 and 404735/2018-5 (GHG), both from Brazil, and also a National Institutes of Health National Institute of Allergy and Infectious Diseases grant (R01AI153356) from the United States (GHG).

References

1. Bongomin, F., et al., *Global and Multi-National Prevalence of Fungal Diseases-Estimate Precision.* J Fungi (Basel), 2017. **3**(4).
2. Brown, G.D., et al., *Hidden killers: human fungal infections.* Sci Transl Med, 2012. **4**(165): p. 165rv13.
3. Alastruey-Izquierdo, A., W.H. Organization, and W.H. Organization, *WHO fungal priority pathogens list to guide research, development and public health action.* 2022.
4. Bertuzzi, M., et al., *Anti-Aspergillus activities of the respiratory epithelium in health and disease.* Journal of Fungi, 2018. **4**(1): p. 8.
5. Baddley, J.W., et al., *Factors associated with mortality in transplant patients with invasive aspergillosis.* Clin Infect Dis, 2010. **50**(12): p. 1559-67.
6. Nivoix, Y., et al., *Factors associated with overall and attributable mortality in invasive aspergillosis.* Clin Infect Dis, 2008. **47**(9): p. 1176-84.
7. Kosmidis, C. and D.W. Denning, *The clinical spectrum of pulmonary aspergillosis.* Thorax, 2015. **70**(3): p. 270-277.
8. Rauseo, A.M., et al., *Hope on the Horizon: Novel Fungal Treatments in Development.* Open Forum Infect Dis, 2020. **7**(2): p. ofaa016.
9. Denning, D.W. and M.J. Bromley, *Infectious Disease. How to bolster the antifungal pipeline.* Science, 2015. **347**(6229): p. 1414-6.
10. Patterson, T.F., et al., *Executive Summary: Practice Guidelines for the Diagnosis and Management of Aspergillosis: 2016 Update by the Infectious Diseases Society of America.* Clin Infect Dis, 2016. **63**(4): p. 433-42.
11. Bongomin, F., et al., *Twelve-month clinical outcomes of 206 patients with chronic pulmonary aspergillosis.* PLoS One, 2018. **13**(4): p. e0193732.
12. Rhodes, J., et al., *Population genomics confirms acquisition of drug-resistant Aspergillus fumigatus infection by humans from the environment.* Nat Microbiol, 2022. **7**(5): p. 663-674.
13. Lestrade, P.P.A., et al., *Triazole resistance in Aspergillus fumigatus: recent insights and challenges for patient management.* Clin Microbiol Infect, 2019. **25**(7): p. 799-806.
14. Steinbach, W.J., D.A. Stevens, and D.W. Denning, *Combination and sequential antifungal therapy for invasive aspergillosis: review of published in vitro and in vivo interactions and 6281 clinical cases from 1966 to 2001.* Clin Infect Dis, 2003. **37 Suppl 3**: p. S188-224.
15. Maertens, J., et al., *Multicenter, noncomparative study of caspofungin in combination with other antifungals as salvage therapy in adults with invasive aspergillosis.* Cancer, 2006. **107**(12): p. 2888-97.
16. Singh, N., et al., *Combination of voriconazole and caspofungin as primary therapy for invasive aspergillosis in solid organ transplant recipients: a prospective, multicenter, observational study.* Transplantation, 2006. **81**(3): p. 320-6.

17. van Rhijn, N., et al., *Antagonism of the Azoles to Olorofim and Cross-Resistance Are Governed by Linked Transcriptional Networks in Aspergillus fumigatus.* mBio, 2022. **13**(6): p. e0221522.
18. Cohen, P., *Protein kinases--the major drug targets of the twenty-first century?* Nat Rev Drug Discov, 2002. **1**(4): p. 309-15.
19. Martin, D.M., D. Miranda-Saavedra, and G.J. Barton, *Kinomer v. 1.0: a database of systematically classified eukaryotic protein kinases.* Nucleic Acids Res, 2009. **37**(Database issue): p. D244-50.
20. Bertuzzi, M., et al., *On the lineage of Aspergillus fumigatus isolates in common laboratory use.* Med Mycol, 2021. **59**(1): p. 7-13.
21. Basenko, E.Y., et al., *FungiDB: An Integrated Bioinformatic Resource for Fungi and Oomycetes.* J Fungi (Basel), 2018. **4**(1).
22. Mistry, J., et al., *Pfam: The protein families database in 2021.* Nucleic Acids Res, 2021. **49**(D1): p. D412-D419.
23. Stamatakis, A., *RAxML version 8: a tool for phylogenetic analysis and post-analysis of large phylogenies.* Bioinformatics, 2014. **30**(9): p. 1312-3.
24. Letunic, I. and P. Bork, *Interactive Tree Of Life (iTOL) v5: an online tool for phylogenetic tree display and annotation.* Nucleic Acids Res, 2021. **49**(W1): p. W293-W296.
25. Zhao, C., et al., *High-Throughput Gene Replacement in Aspergillus fumigatus.* Current Protocols in Microbiology, 2019. **54**(1): p. e88.
26. Wanka, F., et al., *Tet-on, or Tet-off, that is the question: Advanced conditional gene expression in Aspergillus.* Fungal Genet Biol, 2016. **89**: p. 72-83.
27. van Rhijn, N., et al., *Development of a marker-free mutagenesis system using CRISPR-Cas9 in the pathogenic mould Aspergillus fumigatus.* Fungal Genet Biol, 2020. **145**: p. 103479.
28. Van Rhijn, N., *A genome scale census of virulence factors in the major mould pathogen of human lungs, Aspergillus fumigatus.* 2019.
29. Fraczek, M.G., et al., *The cdr1B efflux transporter is associated with non-cyp51a-mediated itraconazole resistance in Aspergillus fumigatus.* Journal of Antimicrobial Chemotherapy, 2013. **68**(7): p. 1486-1496.
30. Kafer, E., *Meiotic and mitotic recombination in Aspergillus and its chromosomal aberrations.* Adv Genet, 1977. **19**: p. 33-131.
31. Johns, A., et al., *A Nonredundant Phosphopantetheinyl Transferase, PptA, Is a Novel Antifungal Target That Directs Secondary Metabolite, Siderophore, and Lysine Biosynthesis in Aspergillus fumigatus and Is Critical for Pathogenicity.* mBio, 2017. **8**(4).
32. Furukawa, T., et al., *Exploring a novel genomic safe-haven site in the human pathogenic mould Aspergillus fumigatus.* Fungal Genet Biol, 2022. **161**: p. 103702.
33. Beck, J., B. Echtenacher, and F. Ebel, *Woronin bodies, their impact on stress resistance and virulence of the pathogenic mould Aspergillus fumigatus and their anchoring at the septal pore of filamentous Ascomycota.* Mol Microbiol, 2013. **89**(5): p. 857-71.

34. Beck, J. and F. Ebel, *Characterization of the major Woronin body protein HexA of the human pathogenic mold Aspergillus fumigatus.* Int J Med Microbiol, 2013. **303**(2): p. 90-7.
35. de Castro, E., et al., *ScanProsite: detection of PROSITE signature matches and ProRule-associated functional and structural residues in proteins.* Nucleic Acids Res, 2006. **34**(Web Server issue): p. W362-5.
36. Jumper, J., et al., *Highly accurate protein structure prediction with AlphaFold.* Nature, 2021. **596**(7873): p. 583-589.
37. Alvarez-Carretero, S., et al., *VSpipe, an Integrated Resource for Virtual Screening and Hit Selection: Applications to Protein Tyrosine Phospahatase Inhibition.* Molecules, 2018. **23**(2).
38. Trott, O. and A.J. Olson, *AutoDock Vina: improving the speed and accuracy of docking with a new scoring function, efficient optimization, and multithreading.* J Comput Chem, 2010. **31**(2): p. 455-61.
39. Borrel, A., et al., *PockDrug: A Model for Predicting Pocket Druggability That Overcomes Pocket Estimation Uncertainties.* J Chem Inf Model, 2015. **55**(4): p. 882-95.
40. De Souza, C.P., et al., *Functional analysis of the Aspergillus nidulans kinome.* PLoS One, 2013. **8**(3): p. e58008.
41. Kosti, I., et al., *Comparative analysis of fungal protein kinases and associated domains.* BMC Genomics, 2010. **11**: p. 133.
42. Miranda-Saavedra, D. and G.J. Barton, *Classification and functional annotation of eukaryotic protein kinases.* Proteins, 2007. **68**(4): p. 893-914.
43. Furukawa, T., et al., *The negative cofactor 2 complex is a key regulator of drug resistance in Aspergillus fumigatus.* Nat Commun, 2020. **11**(1): p. 427.
44. Souza, A.C.O., et al., *Loss of Septation Initiation Network (SIN) kinases blocks tissue invasion and unlocks echinocandin cidal activity against Aspergillus fumigatus.* PLoS Pathog, 2021. **17**(8): p. e1009806.
45. Macdonald, D., et al., *Inducible Cell Fusion Permits Use of Competitive Fitness Profiling in the Human Pathogenic Fungus Aspergillus fumigatus.* Antimicrob Agents Chemother, 2019. **63**(1).
46. Valiante, V., et al., *The MpkA MAP kinase module regulates cell wall integrity signaling and pyomelanin formation in Aspergillus fumigatus.* Fungal Genet Biol, 2009. **46**(12): p. 909-18.
47. Liebmann, B., et al., *The cyclic AMP-dependent protein kinase a network regulates development and virulence in Aspergillus fumigatus.* Infect Immun, 2004. **72**(9): p. 5193-203.
48. Goyard, S., et al., *The Yak1 kinase is involved in the initiation and maintenance of hyphal growth in Candida albicans.* Mol Biol Cell, 2008. **19**(5): p. 2251-66.
49. Garrett, S., M.M. Menold, and J.R. Broach, *The Saccharomyces cerevisiae YAK1 gene encodes a protein kinase that is induced by arrest early in the cell cycle.* Mol Cell Biol, 1991. **11**(8): p. 4045-52.
50. Yang, Q., et al., *Involvement of BcYak1 in the Regulation of Vegetative Differentiation and Adaptation to Oxidative Stress of Botrytis cinerea.* Front Microbiol, 2018. **9**: p. 281.

51. Han, J.H., et al., *Role of the MoYAK1 protein kinase gene in Magnaporthe oryzae development and pathogenicity.* Environ Microbiol, 2015. **17**(11): p. 4672-89.
52. Suwunnakorn, S., et al., *Role of the yakA gene in morphogenesis and stress response in Penicillium marneffei.* Microbiology (Reading), 2014. **160**(Pt 9): p. 1929-1939.
53. Lee, P., et al., *Yeast Yak1 kinase, a bridge between PKA and stress-responsive transcription factors, Hsf1 and Msn2/Msn4.* Mol Microbiol, 2008. **70**(4): p. 882-95.
54. Wang, Z., et al., *A fungal ABC transporter FgAtm1 regulates iron homeostasis via the transcription factor cascade FgAreA-HapX.* PLoS Pathog, 2019. **15**(9): p. e1007791.
55. Gow, N.A., A.J. Brown, and F.C. Odds, *Fungal morphogenesis and host invasion.* Curr Opin Microbiol, 2002. **5**(4): p. 366-71.
56. Ryder, L.S., et al., *A sensor kinase controls turgor-driven plant infection by the rice blast fungus.* Nature, 2019. **574**(7778): p. 423-427.
57. Steinberg, G., et al., *Woronin body-based sealing of septal pores.* Fungal Genet Biol, 2017. **109**: p. 53-55.
58. Proctor, S.A., et al., *Contributions of turgor pressure, the contractile ring, and septum assembly to forces in cytokinesis in fission yeast.* Curr Biol, 2012. **22**(17): p. 1601-8.
59. MacAlpine, J., et al., *A small molecule produced by Lactobacillus species blocks Candida albicans filamentation by inhibiting a DYRK1-family kinase.* Nat Commun, 2021. **12**(1): p. 6151.
60. Fisher, M.C., et al., *Tackling the emerging threat of antifungal resistance to human health.* Nat Rev Microbiol, 2022. **20**(9): p. 557-571.
61. Roemer, T., et al., *Large-scale essential gene identification in Candida albicans and applications to antifungal drug discovery.* Mol Microbiol, 2003. **50**(1): p. 167-81.
62. Giaever, G., et al., *Functional profiling of the Saccharomyces cerevisiae genome.* Nature, 2002. **418**(6896): p. 387-91.
63. Smith, A.M., et al., *Quantitative phenotyping via deep barcode sequencing.* Genome Res, 2009. **19**(10): p. 1836-42.
64. Morogovsky, A., et al., *Horizontal Gene Transfer of Triazole Resistance in Aspergillus fumigatus.* Microbiol Spectr, 2022. **10**(3): p. e0111222.
65. Kurian, S.M., A. Di Pietro, and N.D. Read, *Live-cell imaging of conidial anastomosis tube fusion during colony initiation in Fusarium oxysporum.* PLoS One, 2018. **13**(5): p. e0195634.
66. Roca, M.G., et al., *Cell biology of conidial anastomosis tubes in Neurospora crassa.* Eukaryot Cell, 2005. **4**(5): p. 911-9.
67. Fuller, K.K., et al., *Divergent Protein Kinase A isoforms co-ordinately regulate conidial germination, carbohydrate metabolism and virulence in Aspergillus fumigatus.* Mol Microbiol, 2011. **79**(4): p. 1045-62.
68. Dirr, F., et al., *AfMkk2 is required for cell wall integrity signaling, adhesion, and full virulence of the human pathogen Aspergillus fumigatus.* Int J Med Microbiol, 2010. **300**(7): p. 496-502.

69. Schmelzle, T., et al., *Activation of the RAS/cyclic AMP pathway suppresses a TOR deficiency in yeast.* Mol Cell Biol, 2004. **24**(1): p. 338-51.
70. Lee, P., et al., *Regulation of yeast Yak1 kinase by PKA and autophosphorylation-dependent 14-3-3 binding.* Mol Microbiol, 2011. **79**(3): p. 633-46.
71. Mouriño-Pérez, R.R., *Septum development in filamentous ascomycetes.* Fungal Biology Reviews, 2013. **27**(1): p. 1-9.
72. Bleichrodt, R.J., et al., *Hyphal heterogeneity in Aspergillus oryzae is the result of dynamic closure of septa by Woronin bodies.* Mol Microbiol, 2012. **86**(6): p. 1334-44.
73. Bleichrodt, R.J., et al., *Switching from a unicellular to multicellular organization in an Aspergillus niger hypha.* mBio, 2015. **6**(2): p. e00111.
74. Baldin, C., et al., *Comparative proteomics of a tor inducible Aspergillus fumigatus mutant reveals involvement of the Tor kinase in iron regulation.* Proteomics, 2015. **15**(13): p. 2230-43.
75. Geissel, B., et al., *Azole-induced cell wall carbohydrate patches kill Aspergillus fumigatus.* Nat Commun, 2018. **9**(1): p. 3098.
76. Frost, D., et al., *beta-carboline compounds, including harmine, inhibit DYRK1A and tau phosphorylation at multiple Alzheimer's disease-related sites.* PLoS One, 2011. **6**(5): p. e19264.
77. Torreilles, J., M.C. Guerin, and A. Previero, *[Simple compounds with high pharmacologic potential: beta-carbolines. Origins, syntheses, biological properties].* Biochimie, 1985. **67**(9): p. 929-47.

Figures

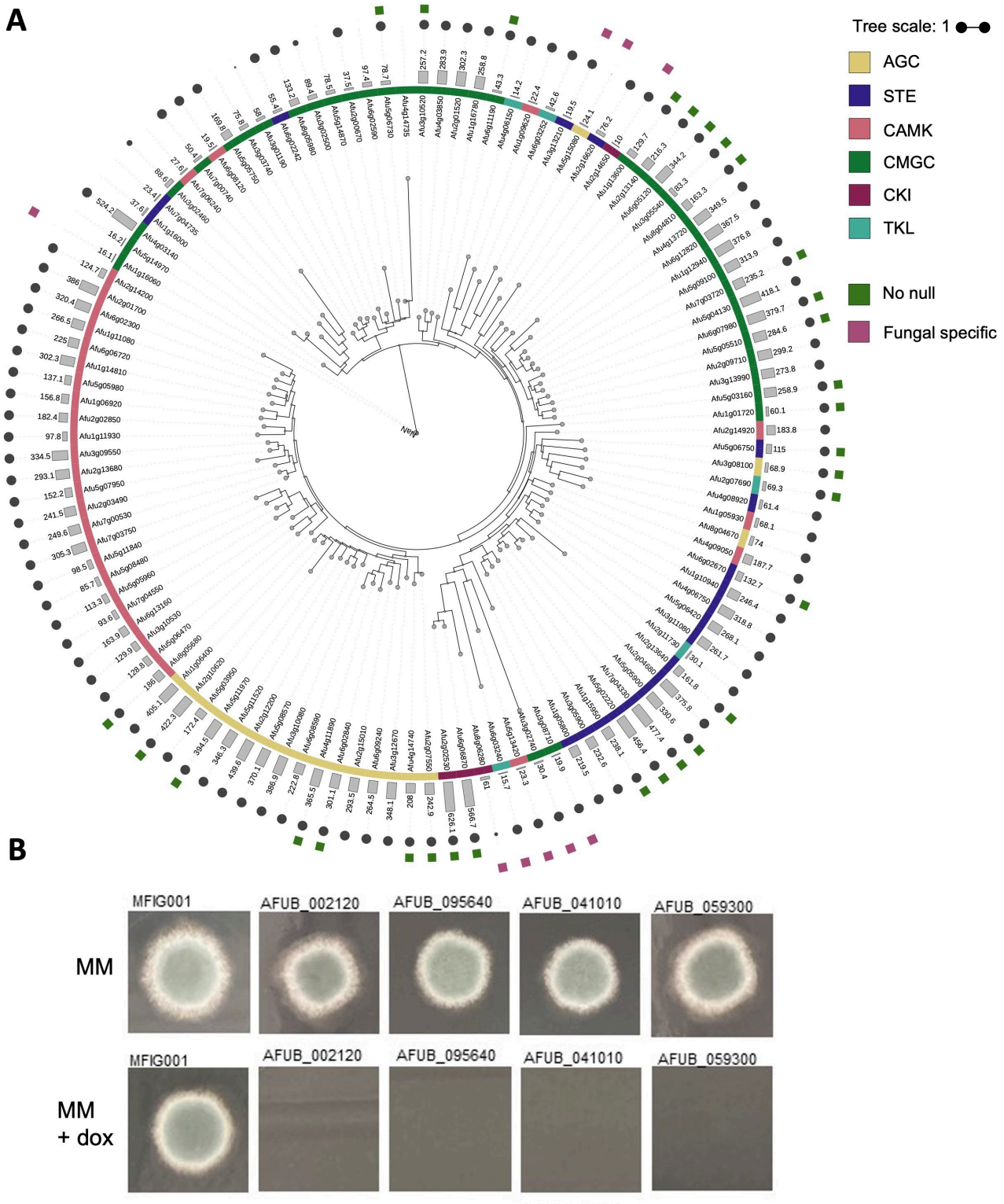


Figure 1

Generation of the kinase knockout collection in *A. fumigatus*. A) A phylogenetic tree (Maximum-likelihood) of the kinases found in Af293. The kinase family (first colour ring), the Kinomer score (barchart), the occurrence of each kinase within the pangenome of *A. fumigatus* (grey circle size), if a homokaryon null was constructed (green squares) and if the kinase is fungal specific (purple square) is shown as annotations around the phylogenetic tree. B) Four potential essential kinases were validated

using a Tet-OFF construct to replace the native promoter. Shutting down expression via addition of doxycycline to the medium resulted in no growth after 72 hours at 37 Celsius, adding further evidence to the essentiality of these kinase for viability.

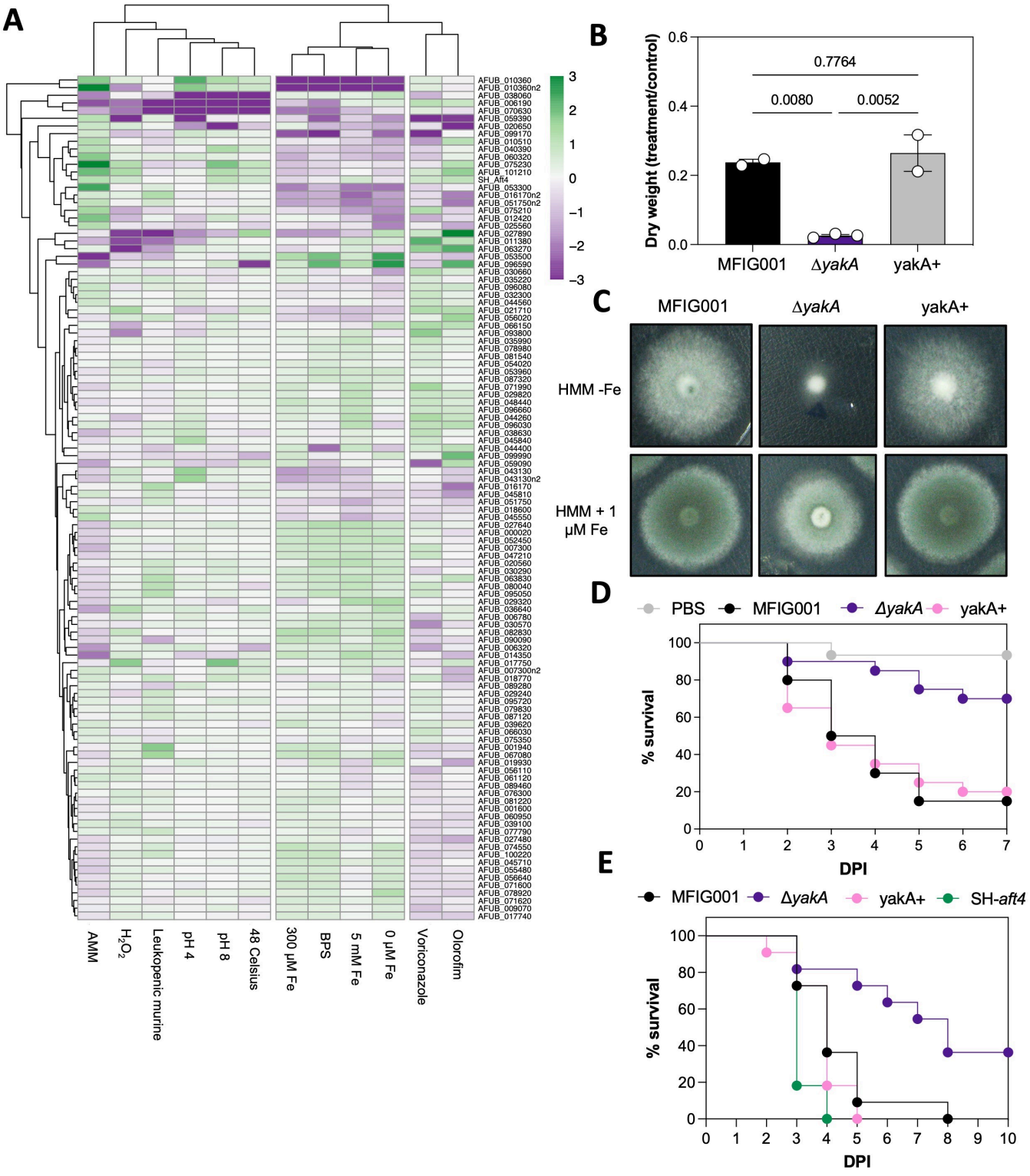


Figure 2

Bar-seq of *A. fumigatus* identifies YakA as a potential novel antifungal target. A) Heatmap of fitness relative to the control condition for each kinase (n = 5). Fitness was calculated by DESeq2 on raw counts.

Heatmap was generated by Pheatmap, full linkage clustering on rows and columns (cutree_cols=2). B) Dry weight was measured after overnight culture in HMM, with and without 0.5 mg/L itraconazole, at 37 Celsius shaking 130 rpm. Statistical difference was assessed by using one-way ANOVA. C) 1000 spores of MFIG001, Δ*yakA* and the reconstituted isolate (yakA+) were spot inoculated on HMM without iron and HMM with 1 μM iron added and incubated for 72 hours at 37 Celsius. D) Survival curves in a *Galleria mello*nella model of aspergillosis. Statistical significance was assessed by Kaplan–Meier survival analysis. E) Survival in a leukopenic murine model of aspergillosis. Statistical difference was assessed by Kaplan–Meier survival analysis.

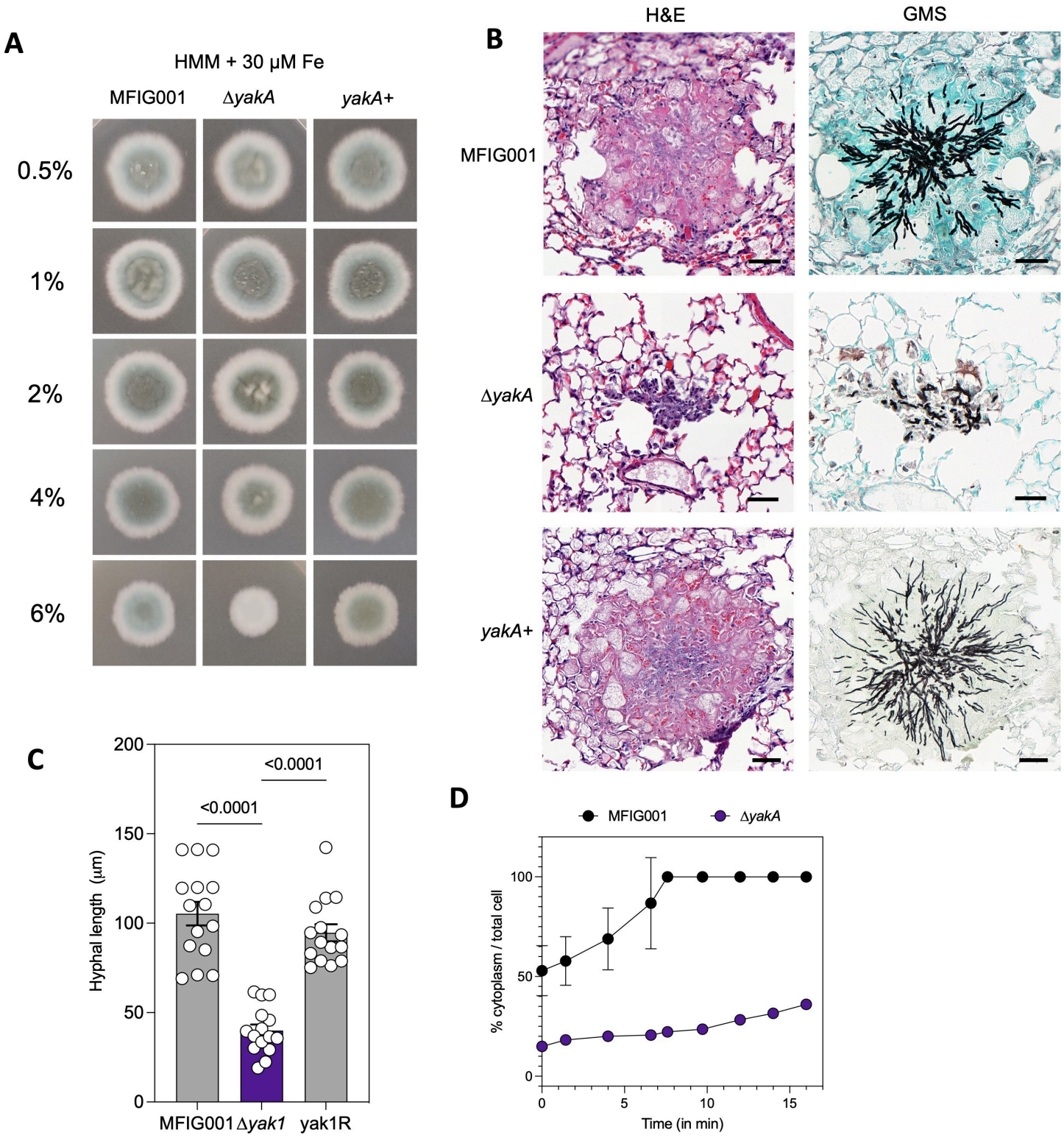


Figure 3

In detail phenotypic analysis of Δ*yakA*. A) 1000 spores of MFIG001, Δ*yakA*, yakA+ were spotted on HMM + 30 µM Fe and imaged after 72 hours at 37 Celsius. An increasing agarose concentration (0.5-6%) was used to make up the HMM medium. B) Representative histological sections of lesions found in murine lungs infected for 3 days with MFIG001, Δ*yakA*and yak+. H&E and GMS stains were performed on neighbouring sections. C) The hyphal length within histological sections (n = 15) was measured.

Statistical difference was assessed by one-way ANOVA. D) Recovery from cytorrhysis after addition of glycerol to the medium. The % cytoplasm compared to the total cell size was measured for individual septal compartments.

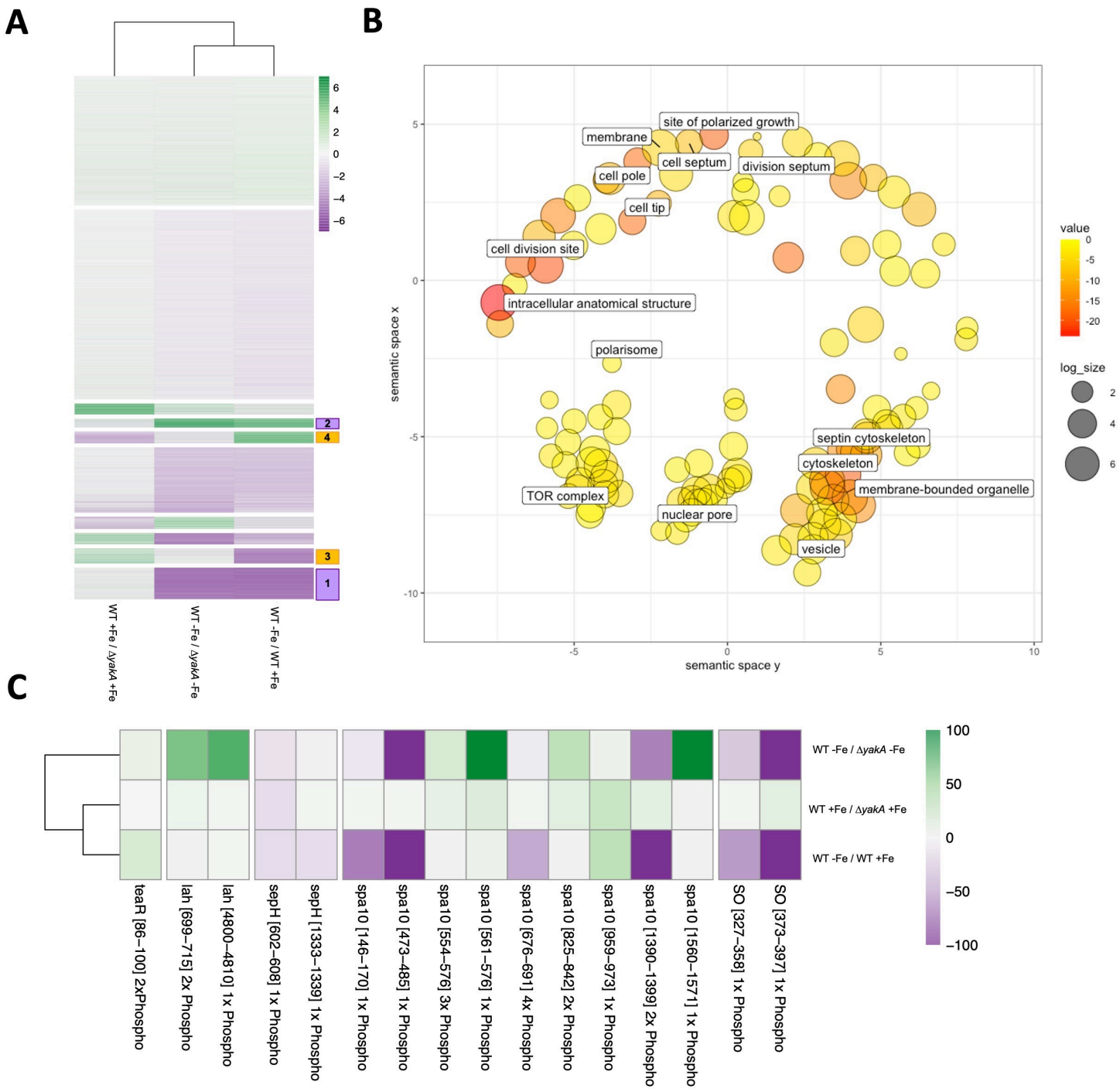


Figure 4

Phosphoproteomics in response to iron limitation. A) Heatmap of phosphopeptides upon iron limitation in MFIG001 and Δ*yakA*. K-means clustering was performed to identify clusters of phosphopeptides differentially phosphorylated dependent upon *yakA* or independent of *yakA*. B) GO-term analysis in Revigo of *yakA*-dependent phosphopeptides in response to iron limitation. Size of circles is the size of

each enrichment category. Colour represents the p-value. C) A detailed analysis of phosphopeptides in components of the septal pore. Only phosphopeptides that are differentially regulated in at least one condition are shown (> 2-fold up or down).

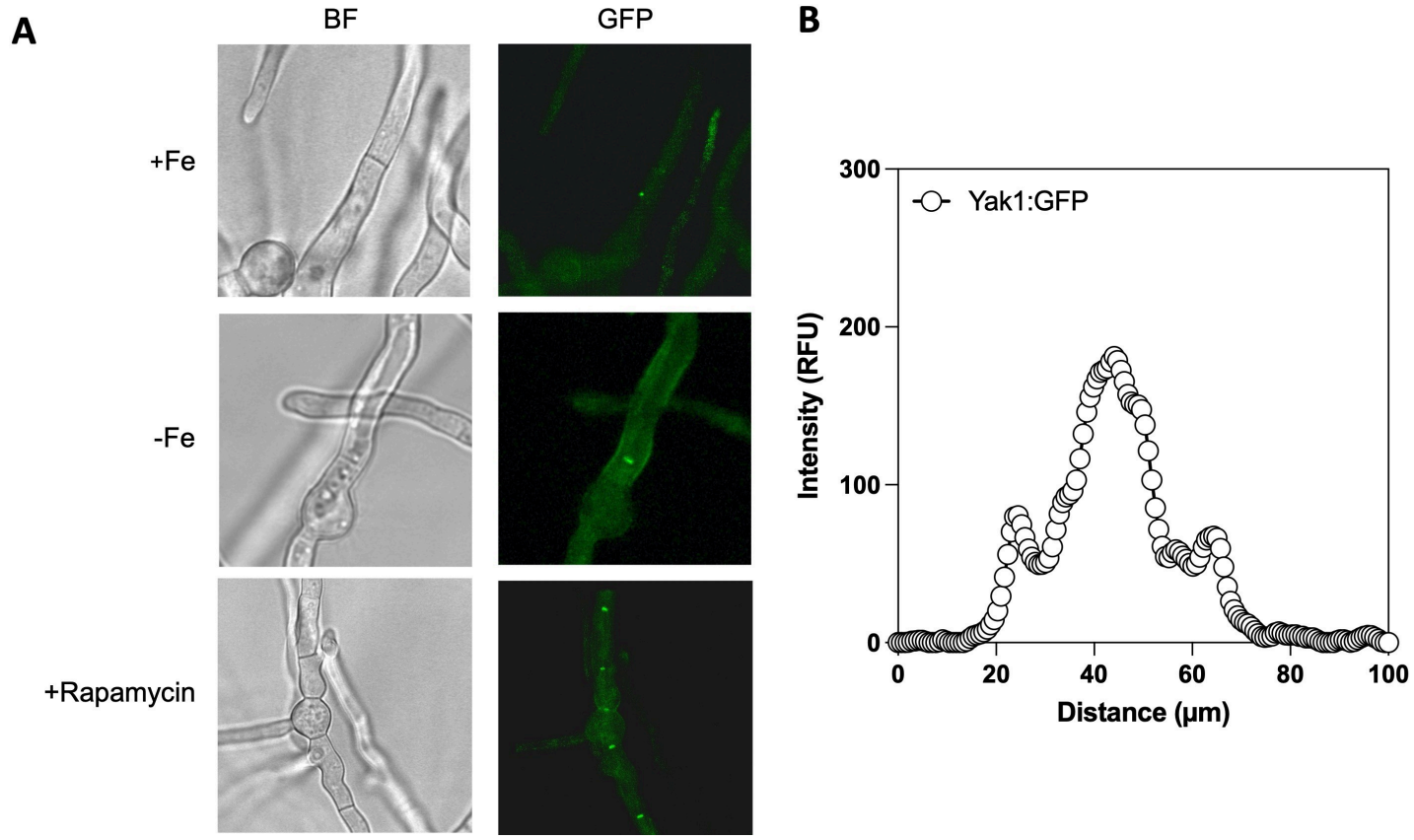


Figure 5

Microscopic analysis of yakA localisation. A) YakA-GFP localisation in control, iron limiting and conditions adding rapamycin. After overnight growth medium was shifted for 1 hour before imaging. Localisation to the septal pore can be observed. B) Quantification of signal through a cross-section of the septum shows higher fluorescent intensity in the central region of the septum, indicating septal pore localisation of YakA-GFP.

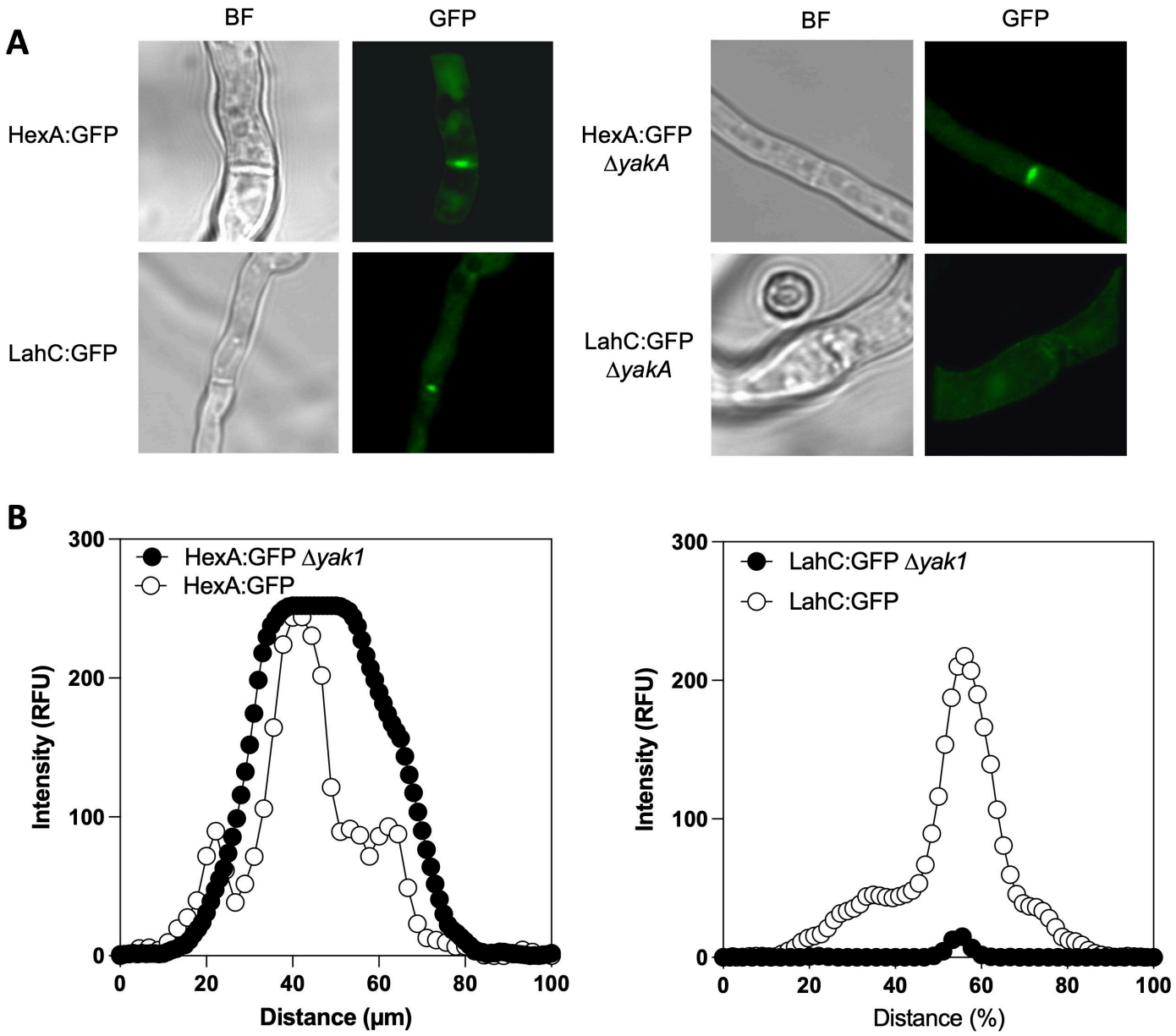


Figure 6

Microscopic characterisation of septal pore components, HexA and Lah. A) Microscopy of single hyphae of HexA-GFP and LacC-GFP upon iron deleted conditions show *yakA*-dependent localisation to the septum or the septal pore. B) Quantification of fluorescent intensity measured across the septum for HexA-GFP and LahC-GFP in the parental isolate or upon deletion of *yakA*.

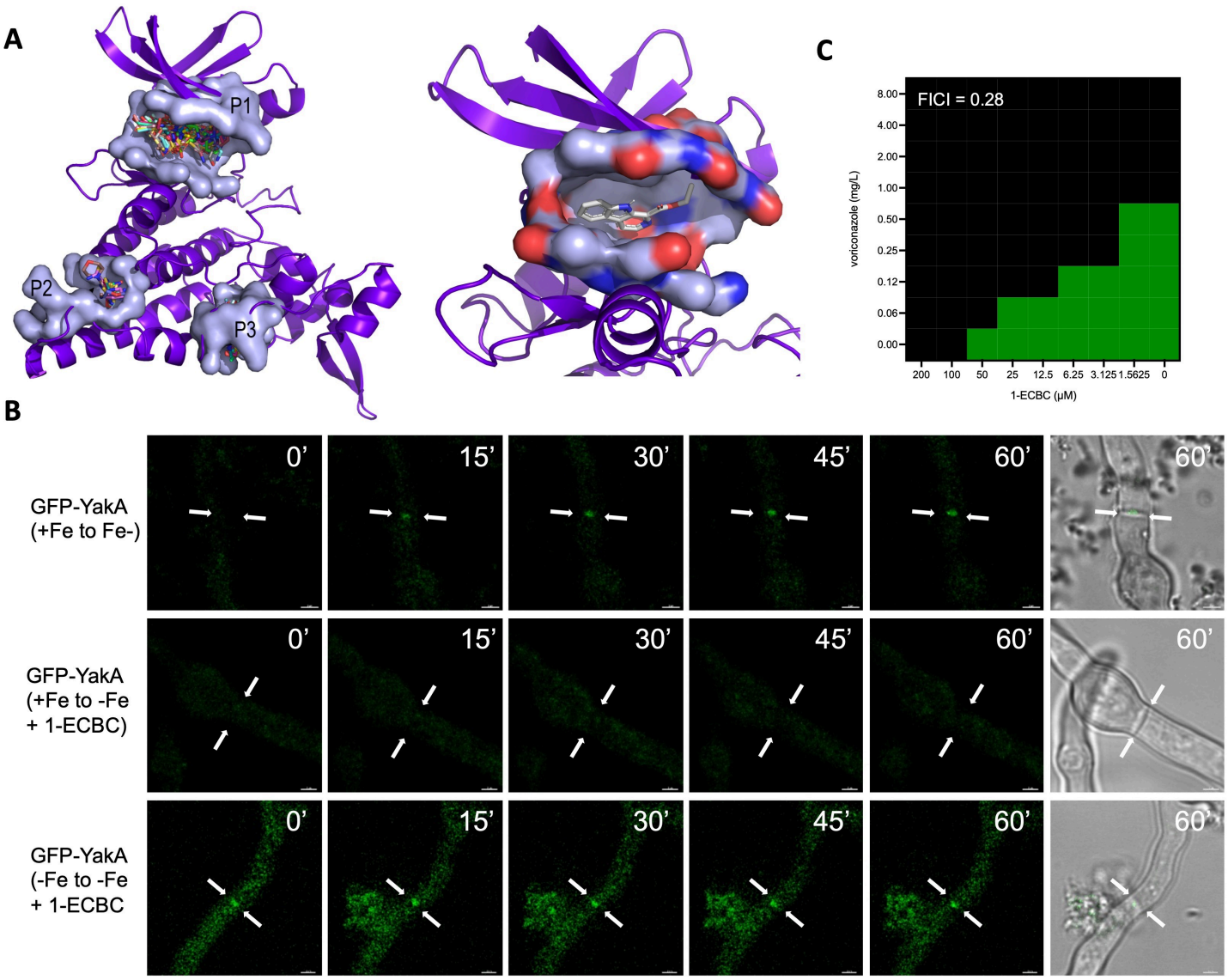


Figure 7

YakA is a druggable target in *A. fumigatus*. A) An alphafold2 model of the YakA protein docked to a library of small molecules. Druggable pockets P1-P3 are shown. Pocket P1 is shown in further detail containing the 1-ECBC molecule. B) Microscopic evaluation of YakA-GFP upon iron limitation and addition of 1-ECBC. Hyphae were followed for one hour upon 1-ECBC addition. C) Checkerboard assay (n=3) for 1-ECBC and voriconazole to assess synergism of these drugs to inhibit growth of *A. fumigatus* MFIG001. The FICI (top-left) was calculated and shown synergism (<0.5).

Supplementary Files

This is a list of supplementary files associated with this preprint. Click to download.

- SupplementalData1.xlsx
- SupplementalData2.xlsx

- SupplementalData3.xlsx
- SupplementalFigures.docx